

Supporting Information

Large-Scale Preparation of Sb³⁺-Activated Hybrid Metal Halides with Efficient Tunable Emission from Visible to Near-Infrared Regions for Advanced Photonics Applications

Ou Xu,[†] Hui Peng,^{†*} Qilin Wei,[‡] Linghang Kong,[†] Xiao Wang,[†] Heng Zhang,[†] Jialong Zhao,[†]
Bingsuo Zou[†]

[†]State Key Laboratory of Featured Metal Materials and Life-cycle Safety for Composite Structures,
MOE Key Laboratory of New Processing Technology for Nonferrous Metals and Materials, and
School of Resources, Environment and Materials, Guangxi University, Nanning 530004, China.

[‡]School of Chemistry and Chemical Engineering, Shandong University, Jinan 250100, China.

Corresponding author: E-mail: penghuimaterial@163.com

Experimental methods

Chemicals: Cadmium chloride (CdCl_2 , 98%), cadmium bromide (CdBr_2 , 98%), tetrapropylamine chloride ($\text{C}_{12}\text{H}_{28}\text{NCl}$, 98%), tetrapropylamine bromide ($\text{C}_{12}\text{H}_{28}\text{NBr}$, 98%), ethyl ether (Et_2O , 99.5%), N, N-Dimethylformamide (DMF, 99.5%), and ethanol (EtOH , 99.5%) were purchased from Sigma-Aldrich. Antimony(III) chloride (SbCl_3 , 99%) and antimony(III) bromide (SbBr_3 , 99.5%) were purchased from Alfa reagent. All materials were used without further processing.

Large-scale preparation of Sb^{3+} -doped $(\text{C}_{12}\text{H}_{28}\text{N})_2\text{CdX}_4$ phosphors: 40 mmol $\text{C}_{12}\text{H}_{28}\text{NCl}$, 20 mmol CdCl_2 , and 3 mmol SbCl_3 were dissolved in 40 mL DMF solution. Afterwards, Et_2O was dropped into the above solution, and Sb^{3+} -doped $(\text{C}_{12}\text{H}_{28}\text{N})_2\text{CdCl}_4$ phosphors can be obtained quickly. For synthesizing Sb^{3+} -doped $(\text{C}_{12}\text{H}_{28}\text{N})_2\text{CdBr}_4$ phosphors, only 30 mmol $\text{C}_{12}\text{H}_{28}\text{NBr}$, 15 mmol CdBr_2 , and 3.75 mmol SbBr_3 were used under otherwise identical conditions. Particularly, the yield of both Sb^{3+} -doped phosphors exceeds 80% based on the total Cd and Sb contents.

Preparation of Sb^{3+} -doped $(\text{C}_{12}\text{H}_{28}\text{N})_2\text{CdCl}_x\text{Br}_{4-x}$ ($x = 0 - 4$) phosphors: The synthesis of Sb^{3+} -doped $(\text{C}_{12}\text{H}_{28}\text{N})_2\text{CdCl}_x\text{Br}_{4-x}$ phosphors is similar to that of Sb^{3+} -doped $(\text{C}_{12}\text{H}_{28}\text{N})_2\text{CdCl}_4$ phosphors, but it is necessary to pay attention to the ratio of Cl to Br in the precursors.

Preparation of $(\text{C}_{12}\text{H}_{28}\text{N})_2\text{CdX}_4$ ($X = \text{Cl}, \text{Br}$) crystals: 1 mmol CdX_2 and 2 mmol $\text{C}_{12}\text{H}_{28}\text{NX}$ were dissolved in 2.5 mL DMF via ultrasound treatment. Subsequently, $(\text{C}_{12}\text{H}_{28}\text{N})_2\text{CdX}_4$ bulk crystals were harvested by diffusing Et_2O into the above solution.

Preparation of WLED: The $(\text{C}_{12}\text{H}_{28}\text{N})_2\text{CdCl}_4:\text{Sb}^{3+}$ powders are evenly mixed with commercial blue phosphors $\text{BaMgAl}_{10}\text{O}_{17}:\text{Eu}^{2+}$, green phosphors $\text{Ba}_2\text{SiO}_4:\text{Eu}^{2+}$, and AB glue, and then the above mixture is coated on the 365 nm LED chip. Before testing, the as-fabricated device should be treated in a vacuum environment at 60 °C for 30 minutes.

Preparation of NIR LED: First, $(\text{C}_{12}\text{H}_{28}\text{N})_2\text{CdBr}_4:\text{Sb}^{3+}$ NIR phosphors were blend with AB glue uniformly. Then, the above mixture was coated on 450 blue LED chip. Before testing, the as-fabricated device should be treated in a vacuum environment at 60 °C for 30 minutes.

Characterization: The crystal structures of the as-synthesized compounds were measured by XtaLAB Synergy instrument. Powder X-ray diffraction (PXRD) patterns were collected using SmartLab SE instrument. The morphology and elemental mapping were performed using a new high-resolution field emission scanning electron microscope (SEM, Philips XL30). Energy-dispersive X-ray spectroscopy (EDS) was measured using Oxford Ultim Max65 instrument. The

Raman spectra were acquired on a confocal Raman imaging system (WITec alpha300 R) at an excitation wavelength of 532 nm laser. X-ray photoelectron spectroscopy (XPS) characterization was performed using an X-ray photoelectron spectrometer (ESCALAB 250XI+) manufactured by Thermo Fisher Scientific. The absorption spectra were carried out using Lambda 750 instrument. PL and PLE spectra were performed using HORIBA Fluorolog-QM spectrograph. PLQY and time-resolved PL spectra were evaluated by Edinburgh FLS 1000 instrument. Variable-temperature PL spectra were collected by HORIBA Fluorolog-QM spectrograph. Power-dependent emission spectra were carried out using Witec alpha300R under 405 nm laser excitation. Thermogravimetric analysis (TGA) was characterized by using a thermogravimetric analyzer DTG-60 manufactured in Shimadzu. Electroluminescence (EL) spectra were obtained using Hopoo HPCS6500 instrument.

Calculation details: All calculations were performed using the plane-wave pseudopotential method implemented in the CASTEP package. The exchange-correlation functional was chosen as the Perdew-Burke-Ernzerhof (PBE) functional within the generalized gradient approximation (GGA). The k-point separation was set as gamma point only in the Brillouin zone leading to corresponding Monkhorst-Pack k-point meshes of $3 \times 3 \times 3$.

Table S1. Crystal data and structure refinement of the title compounds.

Empirical formula	(C ₁₂ H ₂₈ N) ₂ CdCl ₄	(C ₁₂ H ₂₈ N) ₂ CdBr ₄	(C ₁₂ H ₂₈ N) ₂ SbBr ₅	(C ₁₂ H ₂₈ N) ₂ SbCl ₅
Formula weight	626.92	804.72	893.97	671.70
Crystal system	monoclinic	monoclinic	monoclinic	triclinic
Space group	C2/c	C2/c	P21/c	P-1
a/Å	32.768(2)	33.373(7)	18.565(5)	10.6100(2)
b/Å	13.9364(9)	14.437(3)	11.840(3)	10.7418(2)
c/Å	15.0048(9)	14.999(3)	16.708(4)	16.2363(3)
α/°	90°	90°	90°	76.000(2)
β/°	109.9740(2)°	111.357(6)°	103.640(5)°	74.827(2)
γ/°	90°	90°	90°	72.614(2)
Volume/Å ³	6464.2(7)	2299.53(13)	3569.0(16)	1677.22(6)
Z	8	4	4	2
Density (calculated) (g·cm ⁻³)	1.288	1.588	1.330	1.664
Absorption coefficient (mm ⁻¹)	1.020	5.412	1.235	6.385
Data/restraints/parameters	7351/2/287	6875/2/309	8994/0/297	6254/72/296
Goodness of fit on F ²	0.950	0.956	1.026	1.041
Final R indexes [I ≥ 2σ(I)]	R ₁ = 0.0340 wR ₂ = 0.0699	R ₁ = 0.0541 wR ₂ = 0.1050	R ₁ = 0.0230 wR ₂ = 0.0530	R ₁ = 0.0799 wR ₂ = 0.1592
Final R indexes [all data]	R ₁ = 0.0633 wR ₂ = 0.0820	R ₁ = 0.1422 wR ₂ = 0.1343	R ₁ = 0.0255 wR ₂ = 0.0543	R ₁ = 0.1700 wR ₂ = 0.1968

Table S2. Comparison of element concentrations obtained from EDS analysis of $x\%Sb^{3+}$ -doped $(C_{12}H_{28}N)_2CdCl_4$.

Element	5%	10%	15%	20%	25%
Cl (%)	80.44	79.3	79.54	78.92	79.2
Cd (%)	19.07	20.07	19.45	19.5	18.72
Sb (%)	0.49	0.63	1.01	1.58	2.08

Table S3. Comparison of element concentrations obtained from EDS analysis of $x\%Sb^{3+}$ -doped $(C_{12}H_{28}N)_2CdBr_4$.

Element	10%	15%	20%	25%	30%
Br (%)	79.75	80.09	79.1	79.74	78.5
Cd (%)	19.85	18.97	19.6	18.43	18.9
Sb (%)	0.41	0.93	1.3	1.83	2.6

Table S4. The optical properties of pure Sb(III)-based compounds and Sb^{3+} -doped samples.

Compounds	PLE (nm)	PL (nm)	Stokes shift (nm)	PLQY (%)	Decay lifetime (LE)
$(C_{12}H_{28}N)_2SbCl_5$	380	610	230	95.52	5.31 μs
$(C_{12}H_{28}N)_2SbBr_5$	460	675	215	60.82	3.37 μs
$(C_{12}H_{28}N)_2CdCl_4:Sb^{3+}$	350	660	310	85.52	1.70 μs
$(C_{12}H_{28}N)_2CdBr_4:Sb^{3+}$	450	720	270	42.63	0.23 μs

Table S5. Photophysical properties of low-dimensional lead-free metal halides with broadband NIR emission.

Compounds	PLE (nm)	PL (nm)	Stokes shift (nm)	PLQY (%)	Refs.
Bmpip ₂ SnI ₄	370	730	360	35	1
Cs ₂ ZnCl ₄ :Sb ³⁺	316	745	429	69.9	2
Rb ₂ InBr ₅ ·H ₂ O:Sb ³⁺	395	766	160	18.1	3
(C ₈ NH ₁₂) ₆ InBr ₉ ·H ₂ O:Sb ³⁺	355	720	365	35.5	4
(PPZ) ₂ SbCl ₇ ·5H ₂ O	350	720	370	24.7	5
(MTP) ₂ SbBr ₅	450	735	285	5.5	6
Cs ₂ ZnCl ₄ :Sn ²⁺	377	700	323	41	7
(C ₁₃ H ₂₂ N) ₂ Sb ₂ Cl ₈	350	865	515	5	8
(C ₁₀ H ₁₆ N) ₂ Sb ₂ Cl ₈	345	990	645	3	8
(C ₁₆ H ₃₆ P)SbCl ₄	335	1070	735	1	8
(C ₁₂ H ₂₈ N) ₂ CdBr ₄ :Sb ³⁺	450	720	270	42.6	This work

Table S6. Comparison of the bond lengths of (C₁₂H₂₈N)₂SbX₅ and Sb³⁺-doped (C₁₂H₂₈N)₂CdX₄ in the ground state and excited state.

(C ₁₂ H ₂₈ N) ₂ SbCl ₅						
	Sb-Cl1(Å)	Sb-Cl2(Å)	Sb-Cl3(Å)	Sb-Cl4(Å)	Sb-Cl5(Å)	Δd
Ground state	2.412	2.675	2.653	2.605	2.650	1.364×10 ⁻³
Excited state	2.412	2.673	2.651	2.606	2.651	1.362×10 ⁻³
(C ₁₂ H ₂₈ N) ₂ SbBr ₅						
	Sb-Br1(Å)	Sb-Br2(Å)	Sb-Br3(Å)	Sb-Br4(Å)	Sb-Br5(Å)	Δd
Ground state	2.562	2.851	2.855	2.768	2.806	1.517×10 ⁻³
Excited state	2.589	2.846	2.831	2.760	2.787	1.105×10 ⁻³
Sb ³⁺ -doped (C ₁₂ H ₂₈ N) ₂ CdCl ₄						
	Sb-Cl1(Å)	Sb-Cl2(Å)	Sb-Cl3(Å)	Sb-Cl4(Å)	Δd	
Ground state	2.593	2.733	2.643	2.533	6.239×10 ⁻⁴	
Excited state	3.108	2.504	2.596	2.697	5.735×10 ⁻³	
Sb ³⁺ -doped (C ₁₂ H ₂₈ N) ₂ CdBr ₄						
	Sb-Br1(Å)	Sb-Br2(Å)	Sb-Br3(Å)	Sb-Br4(Å)	Δd	
Ground state	2.869	2.757	2.849	2.683	5.717×10 ⁻⁴	
Excited state	3.268	2.817	2.654	2.807	5.054×10 ⁻³	

Table S7. Comparison of bond angles of $(C_{12}H_{28}N)_2SbX_5$ and Sb^{3+} -doped $(C_{12}H_{28}N)_2CdX_4$ in the ground state and excited state.

$(C_{12}H_{28}N)_2SbCl_5$									
	Cl1- Sb-	Cl1- Sb-	Cl1- Sb-	Cl1- Sb-	Cl2- Sb-	Cl3- Sb-	Cl5- Sb-	Cl4- Sb-	σ^2
	Cl2(°)	Cl3(°)	Cl4(°)	Cl5(°)	Cl4(°)	Cl2(°)	Cl3(°)	Cl5(°)	
Ground state	88.768	92.831	84.641	91.346	88.060	90.532	93.098	88.778	7.885
Excited state	84.639	91.387	88.609	92.753	93.167	88.732	87.945	90.631	8.062
$(C_{12}H_{28}N)_2SbBr_5$									
	Br1- Sb-	Br1- Sb-	Br1- Sb-	Br1- Sb-	Br2- Sb-	Br3- Sb-	Br5- Sb-	Br4- Sb-	σ^2
	Br2(°)	Br3(°)	Br4(°)	Br5(°)	Br4(°)	Br2(°)	Br3(°)	Br5(°)	
Ground state	91.196	92.175	94.682	89.314	88.276	91.036	87.848	92.690	6.352
Excited state	89.143	94.266	93.947	90.044	88.854	90.035	86.673	94.215	9.238
Sb^{3+} -doped $(C_{12}H_{28}N)_2CdCl_4$									
	Cl1-Sb- Cl2(°)	Cl1-Sb- Cl3(°)	Cl1-Sb- Cl4(°)	Cl2-Sb- Cl4(°)	Cl3-Sb- Cl2(°)	Cl3-Sb- Cl4(°)	σ^2		
Ground state	100.987	109.005	111.464	106.787	113.771	113.954	24.371		
Excited state	81.189	108.694	110.386	137.145	102.881	94.879	466.594		
Sb^{3+} -doped $(C_{12}H_{28}N)_2CdBr_4$									
	Br1-Sb- Br2(°)	Br1-Sb- Br3(°)	Br1-Sb- Br4(°)	Br2-Sb- Br4(°)	Br3-Sb- Br2(°)	Br3-Sb- Br4(°)	σ^2		
Ground state	105.431	103.042	109.704	109.004	109.744	118.718	28.653		
Excited state	82.478	106.702	106.827	95.968	141.989	105.6692	398.229		

Evaluation of metal halide configuration distortion:

The deformation parameters (Δd) and the magnitude of polyhedron angle variance (σ^2) of $[\text{SbCl}_5]^{2-}$ units are used to evaluate the degree of metal halide configuration distortions, and their values can be calculated by the following equations:

$(\text{C}_{25}\text{H}_{22}\text{P})_2\text{SbX}_5$ single crystals:

$$\Delta d = \frac{1}{6} \sum_{n=1}^6 \left(\frac{d_n - d_{ave}}{d_{ave}} \right)^2 \quad (1)$$

$$\sigma^2 = \frac{1}{11} \sum_{i=1}^{12} (\alpha_i - 90^\circ)^2 \quad (2)$$

Sb^{3+} -doped $(\text{C}_{25}\text{H}_{22}\text{P})\text{SbX}_4$ single crystals:

$$\Delta d = \frac{1}{4} \sum_{n=1}^4 \left(\frac{d_n - d_{ave}}{d_{ave}} \right)^2 \quad (3)$$

$$\sigma^2 = \frac{1}{4} \sum_{i=1}^5 (\alpha_i - 90^\circ)^2 \quad (4)$$

where d_{ave} is the average Sb-Cl bond length, d_n denotes the distances of Sb-Cl bonds, and α_i represents the angle of Cl-Sb-Cl.

Note: Tables S6 and S7 exhibit the Sb-X bond lengths and X-Sb-X bond angles of $(\text{C}_{12}\text{H}_{28}\text{N})_2\text{SbX}_5$ and Sb^{3+} -doped $(\text{C}_{12}\text{H}_{28}\text{N})_2\text{CdX}_4$ ($X = \text{Cl}, \text{Br}$) in the ground state and excited state, respectively. The bond length deformation (Δd) and the bond angle variance (σ^2) in the ground state and excited state of $(\text{C}_{12}\text{H}_{28}\text{N})_2\text{SbX}_5$ and Sb^{3+} -doped $(\text{C}_{12}\text{H}_{28}\text{N})_2\text{CdX}_4$ were calculated in Tables S6 and S7. Moreover, the excited state lattice distortion degree (η and w) was calculated via the following equation:

$$\eta = \left| \frac{\Delta d_{ES} - \Delta d_{GS}}{\Delta d_{GS}} \right| \times 100\% \quad (5)$$

$$w = \left| \frac{\sigma_{ES}^2 - \sigma_{GS}^2}{\sigma_{GS}^2} \right| \times 100\% \quad (6)$$

where Δd_{ES} and Δd_{GS} are the bond length deformation (Δd) in the ground state and excited state, respectively. $\Delta \sigma_{ES}^2$ and $\Delta \sigma_{GS}^2$ are the bond angle variance in the ground state and excited state, respectively. Here, the calculated η of $(\text{C}_{12}\text{H}_{28}\text{N})_2\text{SbCl}_5$, $(\text{C}_{12}\text{H}_{28}\text{N})_2\text{SbBr}_5$, Sb^{3+} -doped $(\text{C}_{12}\text{H}_{28}\text{N})_2\text{CdCl}_4$, and Sb^{3+} -doped $(\text{C}_{12}\text{H}_{28}\text{N})_2\text{CdBr}_4$ are 0.15%, 27.16%, 819.22%, and 784.03%, respectively, and the calculated w of $(\text{C}_{12}\text{H}_{28}\text{N})_2\text{SbCl}_5$, $(\text{C}_{12}\text{H}_{28}\text{N})_2\text{SbBr}_5$, Sb^{3+} -doped $(\text{C}_{12}\text{H}_{28}\text{N})_2\text{CdCl}_4$, and Sb^{3+} -doped $(\text{C}_{12}\text{H}_{28}\text{N})_2\text{CdBr}_4$ are 2.24%, 45.43%, 1814.55%, and 1289.83%, respectively. Clearly, the values of η and w for the Sb^{3+} -doped Cd(II)-based compounds are much larger than pure Sb(III)-based metal halides, which leads to a larger Stokes shift of Sb^{3+} -doped Cd(II)-based compounds, and further enables us to obtain NIR emission.

Table S8. PLE band, PL band, output power, and photoelectric conversion efficiency of recently reported low-dimensional metal halides and oxide phosphors with NIR emission.

Compounds	PLE band (nm)	PL band (nm)	Output power (mW)	Photoelectric conversion efficiency (%)	Ref
(C ₂₀ H ₂₀ P) ₂ MnCl ₄ :Sb ³⁺	400	718	13.35	2.6	9
(C ₂₀ H ₂₀ P) ₂ ZnCl ₄ :Sb ³⁺	400	702	15.9	2.7	9
(C ₂₀ H ₂₀ P) ₂ CdCl ₄ :Sb ³⁺	400	705	12.3	2.4	9
Cs ₂ ZnCl ₄ :Sb ³⁺	316	745	27.2	2.9	2
BaAl ₄ Sb ₂ O ₁₂ :Cr ³⁺	425	750	27.15	13.39	10
LiInSi ₂ O ₆ :Cr ³⁺	460	840	51.6	17.2	11
Ga ₃ Al ₃ Ge ₂ O ₁₃ :Cr ³⁺	430	816	34.95	12.8	12
Ca ₄ HfGe ₃ O ₁₂ :Cr ³⁺	460	840	40	7	13
Ca _{3.2} Zn _{0.8} HfGe ₃ O ₁₂ :Cr ³⁺	450	890/1220	55	5.56	14
Ca _{1.8} Mg _{1.2} Al ₂ Ge ₃ O ₁₂ :Cr ³⁺	449	806	12.19	1.9	15
Ba ₃ GeO ₄ Br ₂ :Eu ²⁺	450	685	30.1	22	16
Ba ₃ Lu(BO ₃) ₃ :Eu ²⁺	450	720	4.7	11.6	17
SrY ₂ O ₄ :Eu ²⁺	450	773	38.53	-	18
K ₃ LuSi ₂ O ₇ :Eu ²⁺	460	740	25.12	-	19
(C ₁₂ H ₂₈ N) ₂ CdBr ₄ :Sb ³⁺	450	720	52.92	17.76	This work



Figure S1. Physical image of the as-synthesized $(C_{12}H_{28}N)_2CdCl_4:15\%Sb^{3+}$ phosphors.

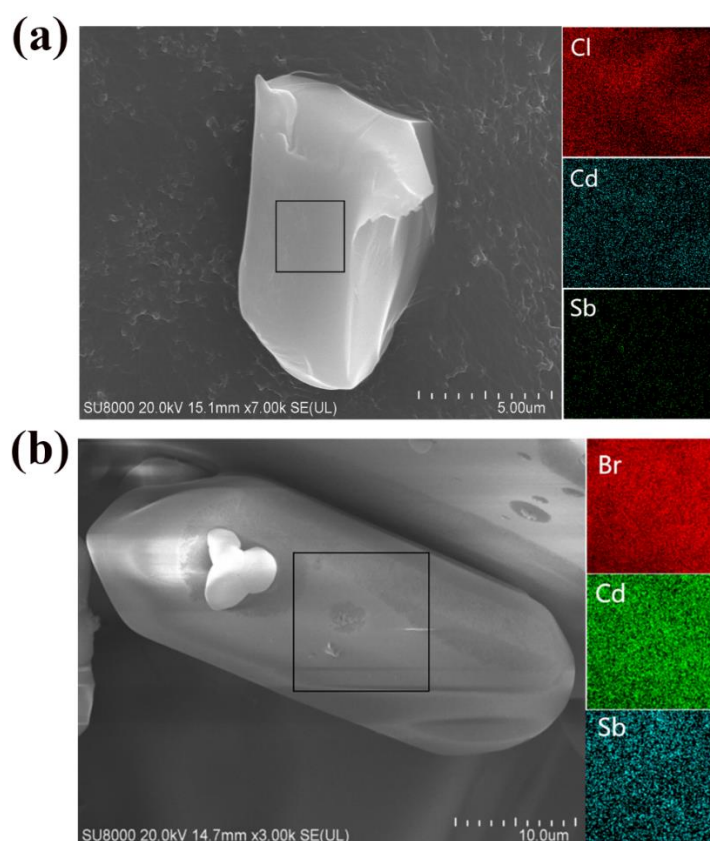


Figure S2. (a) SEM image of $(C_{12}H_{28}N)_2CdCl_4:25\%Sb^{3+}$ and the element mapping images of Cl, Cd, and Sb, respectively. (b) SEM image of $(C_{12}H_{28}N)_2CdBr_4:15\%Sb^{3+}$ and the element mapping images of Br, Cd, and Sb, respectively.

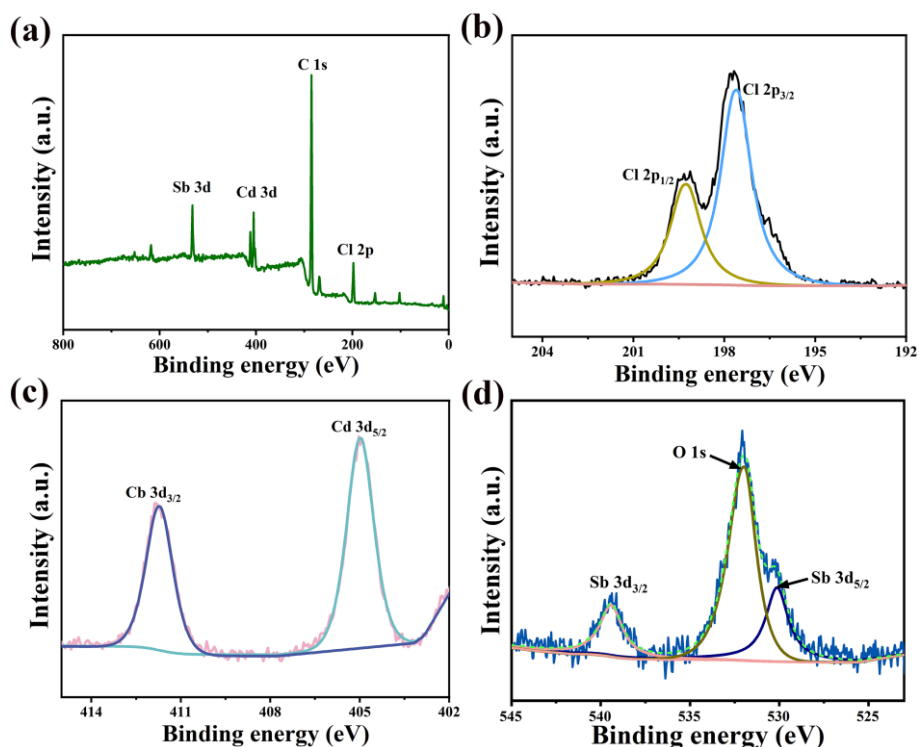


Figure S3. (a) X-ray photoelectron spectroscopic (XPS) analysis of $(\text{C}_{12}\text{H}_{28}\text{N})_2\text{CdCl}_4:15\%\text{Sb}^{3+}$ and the corresponding high-resolution XPS spectra of (b) Cl 3d, (c) Cd 3d, and (d) Sb 3d, respectively.

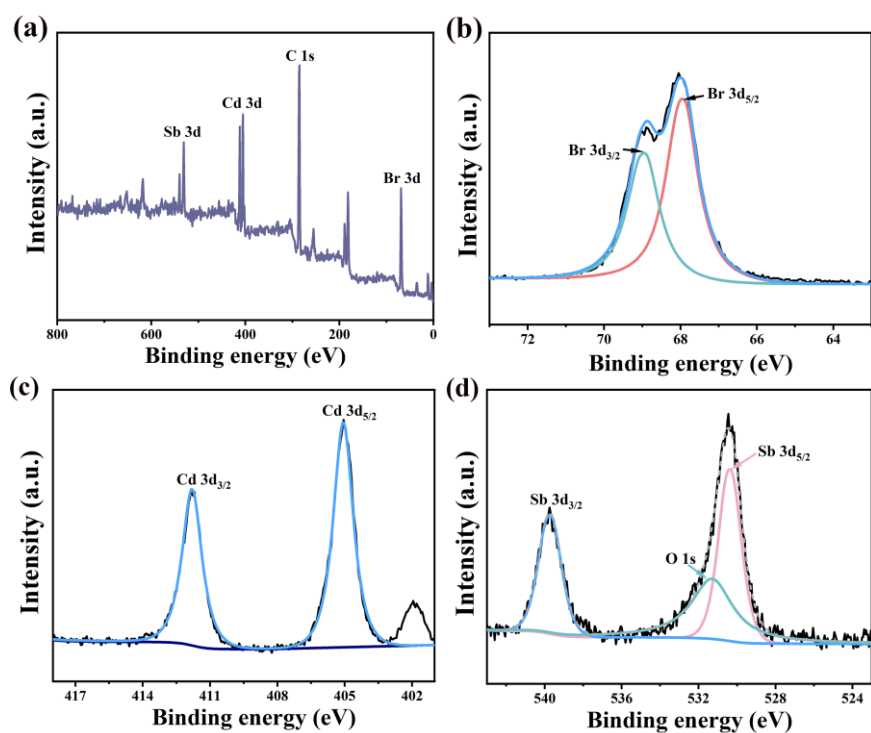


Figure S4. (a) X-ray photoelectron spectroscopic (XPS) analysis of $(\text{C}_{12}\text{H}_{28}\text{N})_2\text{CdBr}_4:25\%\text{Sb}^{3+}$ and the corresponding high-resolution XPS spectra of (b) Br 3d, (c) Cd 3d, and (d) Sb 3d, respectively.

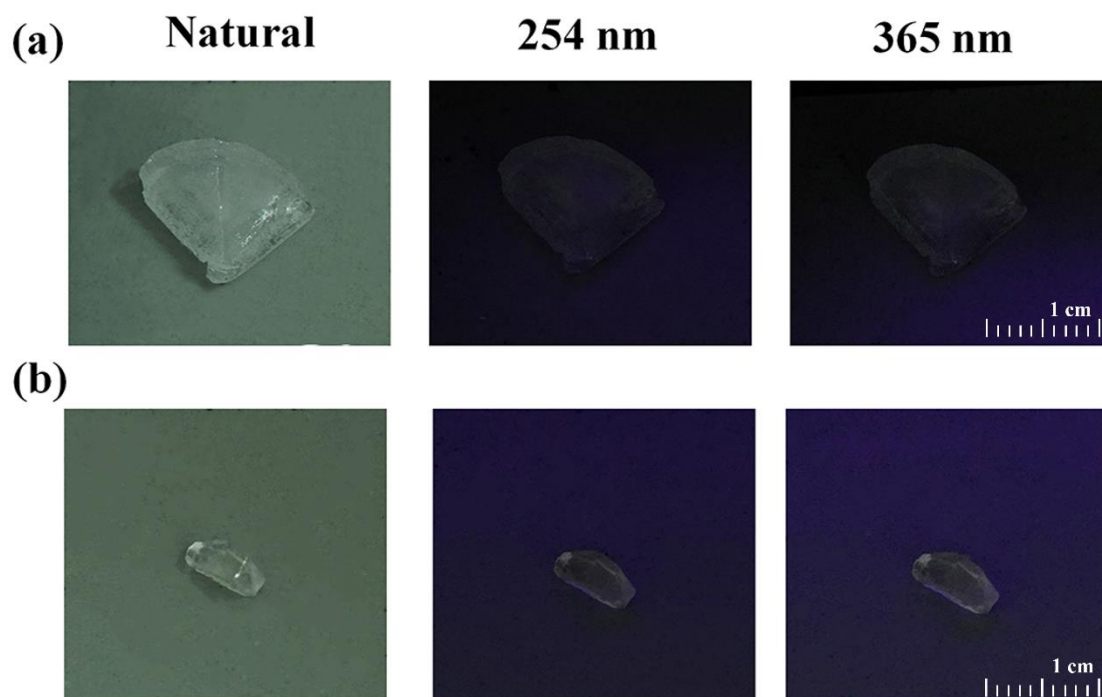


Figure S5. The optical photographs of (a) $(C_{12}H_{28}N)_2CdCl_4$ and (b) $(C_{12}H_{28}N)_2CdBr_4$ under 254 and 365 nm excitation, respectively.

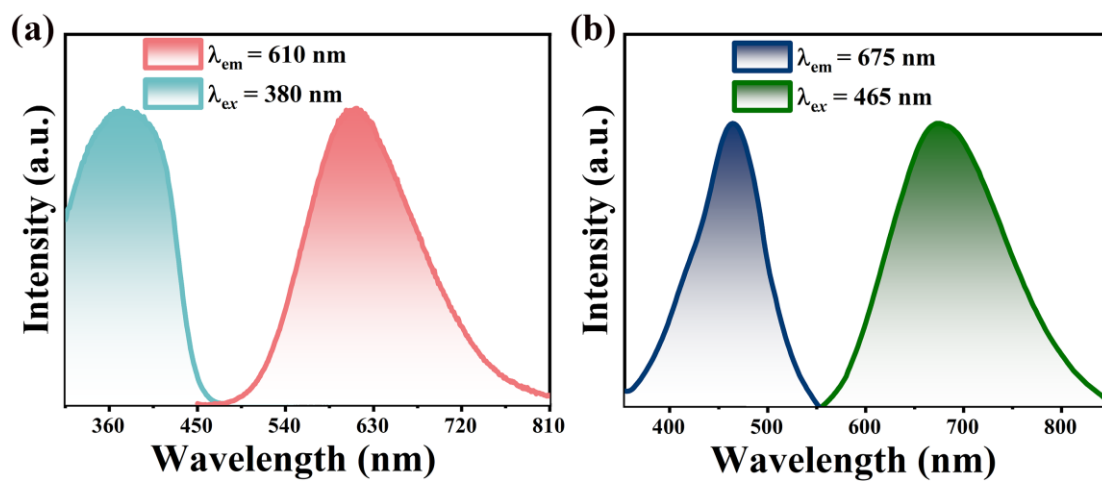


Figure S6. PLE and PL spectra of (a) $(C_{12}H_{28}N)_2SbCl_5$ and (b) $(C_{12}H_{28}N)_2SbBr_5$.

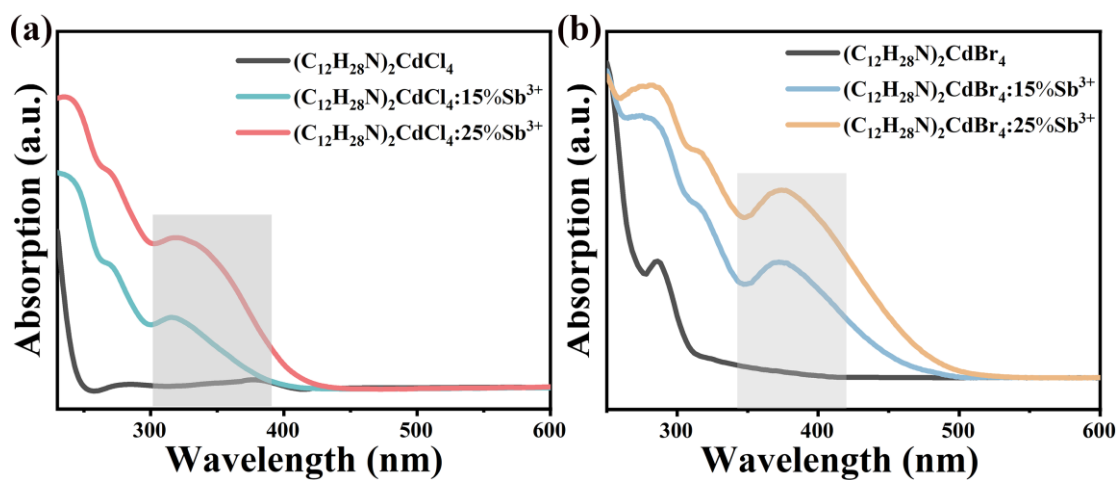


Figure S7. (a) The absorption spectra pristine and Sb^{3+} -doped $(\text{C}_{12}\text{H}_{28}\text{N})_2\text{CdCl}_4$. (b) The absorption spectra pristine and Sb^{3+} -doped $(\text{C}_{12}\text{H}_{28}\text{N})_2\text{CdBr}_4$.

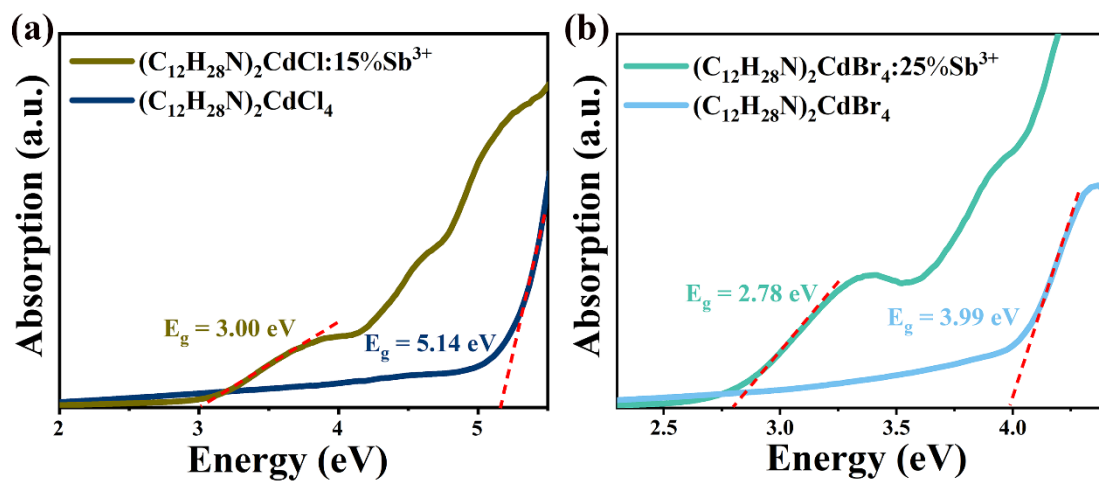


Figure S8. (a) The bandgap of pristine and Sb^{3+} -doped $(\text{C}_{12}\text{H}_{28}\text{N})_2\text{CdCl}_4$. (b) The bandgap of pristine and Sb^{3+} -doped $(\text{C}_{12}\text{H}_{28}\text{N})_2\text{CdBr}_4$.

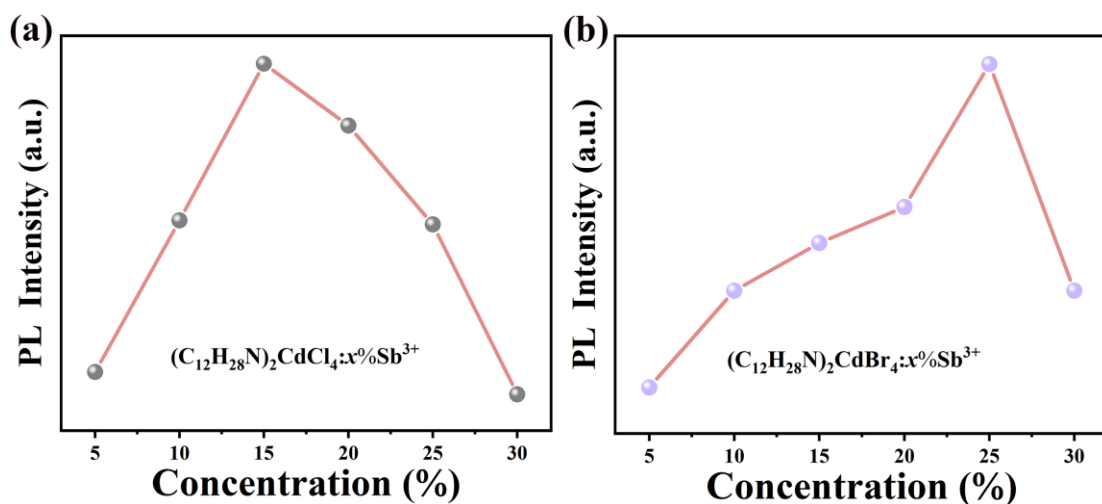


Figure S9. PL intensity (a) $(C_{12}H_{28}N)_2CdCl_4$ and (b) $(C_{12}H_{28}N)_2CdBr_4$ under various Sb^{3+} doping contents.

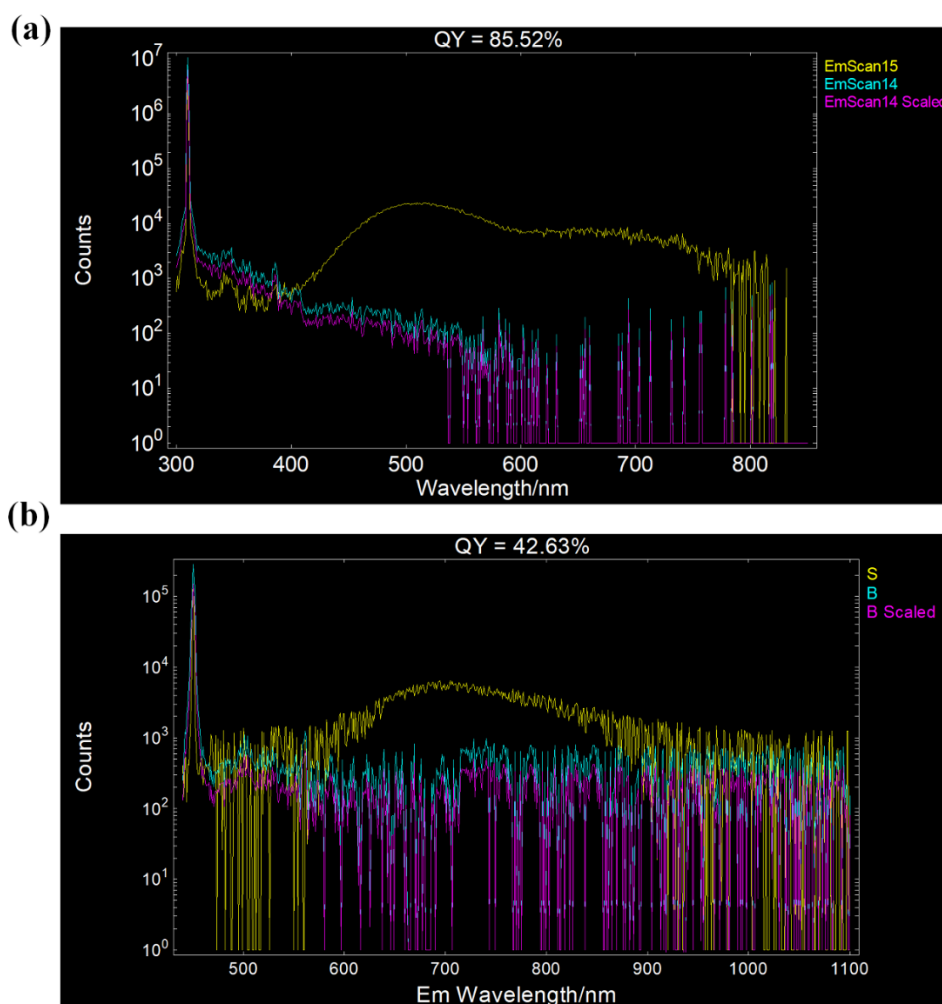


Figure S10. PLQY of (a) 15% Sb^{3+} -doped $(C_{12}H_{28}N)_2CdCl_4$ and (b) 25% Sb^{3+} -doped $(C_{12}H_{28}N)_2CdBr_4$.

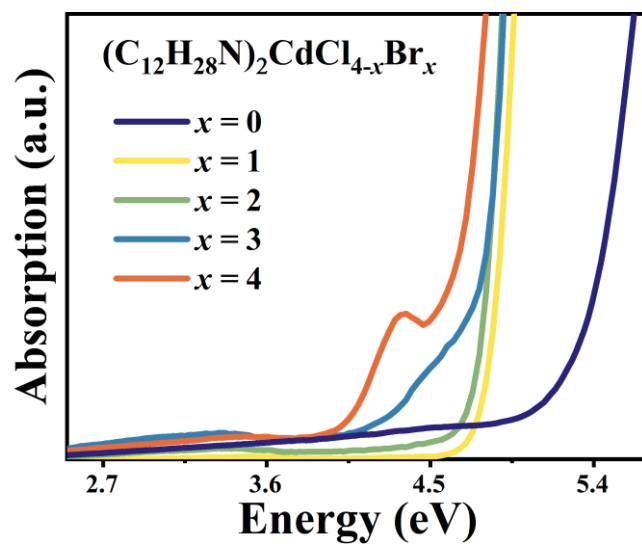


Figure S11. The bandgap of Sb^{3+} -doped $(C_{12}H_{28}N)_2CdCl_{4-x}Br_x$ phosphors with different Cl/Br ratios.

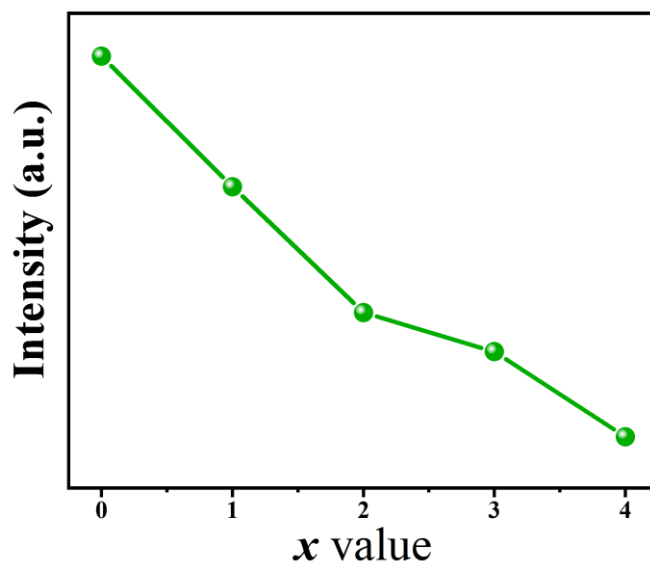


Figure S12. The emission intensity of $(C_{12}H_{28}N)_2CdCl_{4-x}Br_x$ with different Cl/Br ratios.

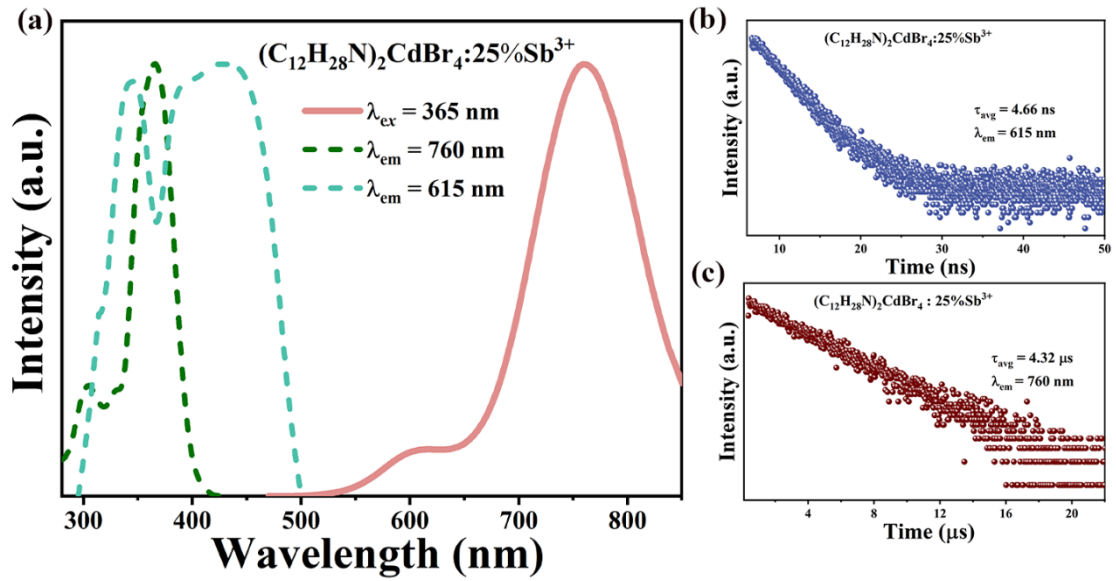


Figure S13. (a) PLE and PL spectra of $(\text{C}_{12}\text{H}_{28}\text{N})_2\text{CdBr}_4:25\%\text{Sb}^{3+}$ at 80 K. PL decay lifetimes of $(\text{C}_{12}\text{H}_{28}\text{N})_2\text{CdBr}_4:25\%\text{Sb}^{3+}$ monitored at (b) 615 nm emission and (c) 760 nm emission at 80 K.

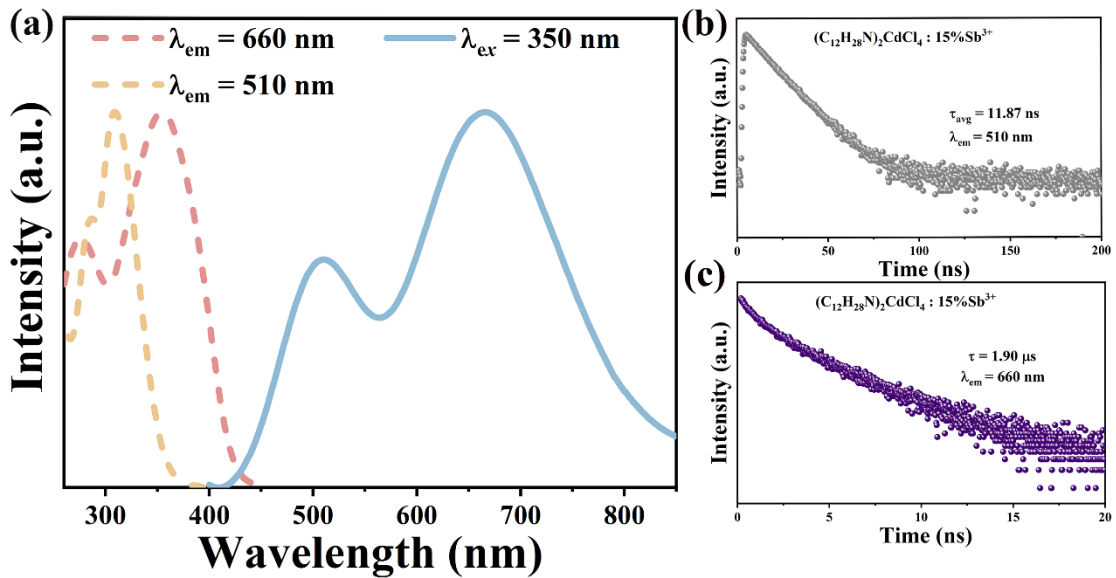


Figure S14. (a) RT PLE and PL spectra of $(\text{C}_{12}\text{H}_{28}\text{N})_2\text{CdCl}_4:15\%\text{Sb}^{3+}$. RT PL decay lifetimes of $(\text{C}_{12}\text{H}_{28}\text{N})_2\text{CdCl}_4:15\%\text{Sb}^{3+}$ monitored at (b) 510 nm and (c) 660 nm.

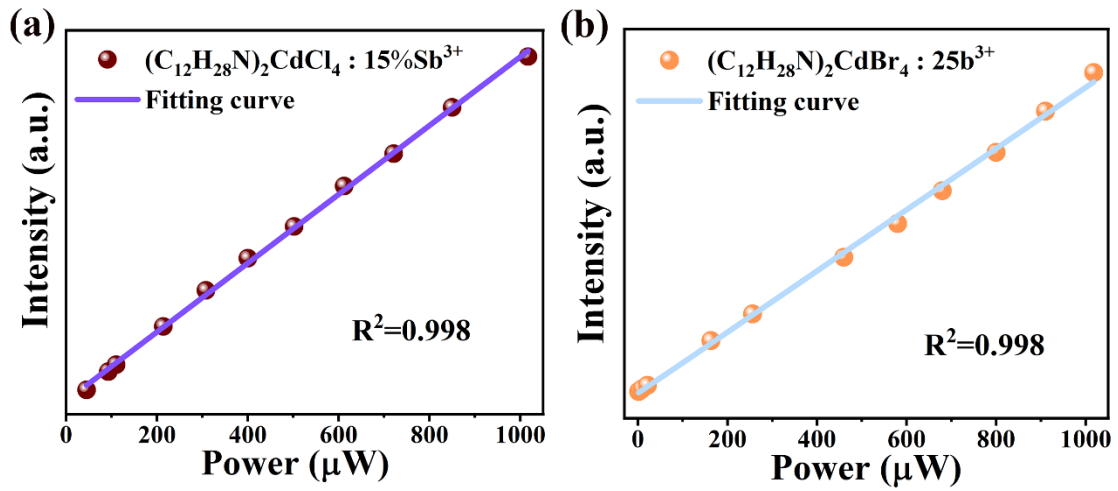


Figure S15. The PL intensity of (a) $(\text{C}_{12}\text{H}_{28}\text{N})_2\text{CdCl}_4:15\%\text{Sb}^{3+}$ and $(\text{C}_{12}\text{H}_{28}\text{N})_2\text{CdBr}_4:25\%\text{Sb}^{3+}$ under various excitation powers (405 nm laser excitation).

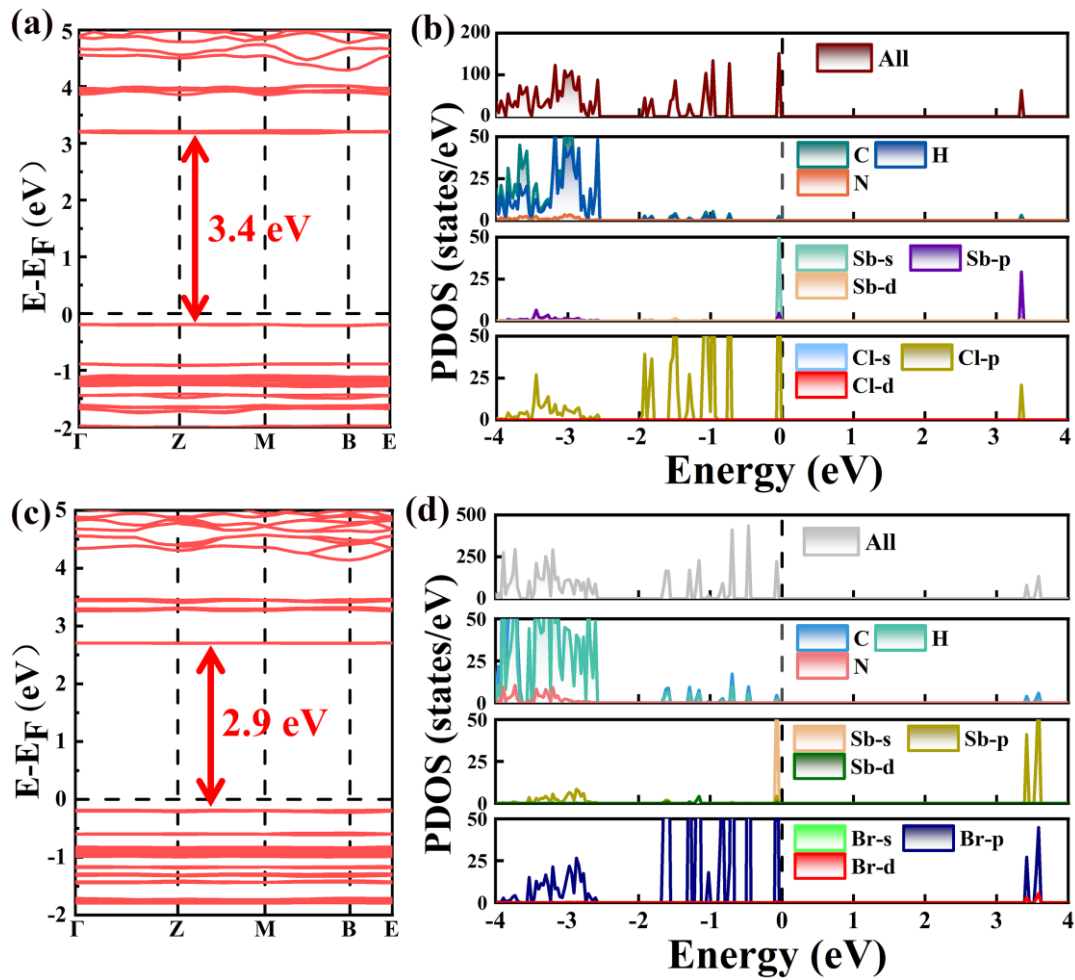


Figure S16. Band structure and partial DOS of (a, b) $(\text{C}_{12}\text{H}_{28}\text{N})_2\text{SbCl}_5$ and (c, d) $(\text{C}_{12}\text{H}_{28}\text{N})_2\text{SbBr}_5$.

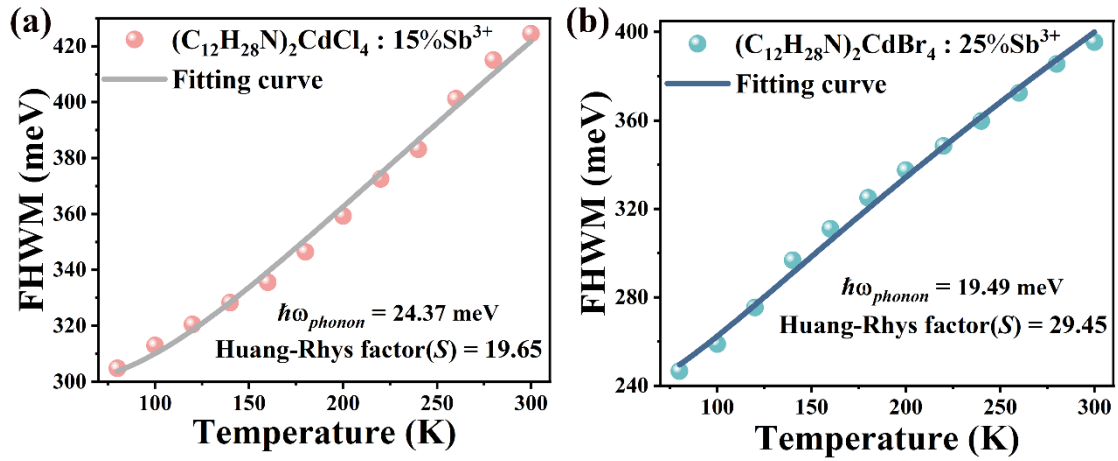


Figure S17. The fitted Huang-Rhys factor (S) of (a) $(C_{12}H_{28}N)_2CdCl_4:15\%Sb^{3+}$ and (b) $(C_{12}H_{28}N)_2CdBr_4:25\%Sb^{3+}$.

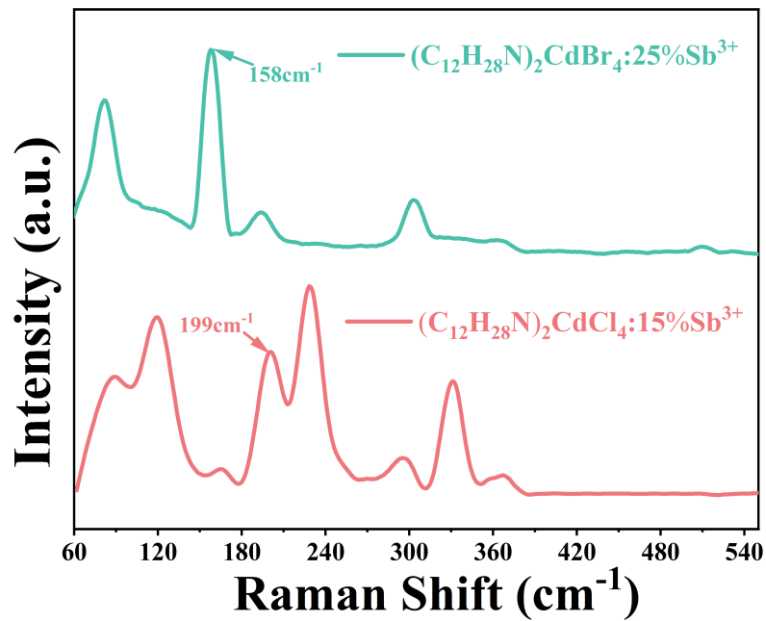


Figure S18. The Raman spectra of $(C_{12}H_{28}N)_2CdCl_4:15\%Sb^{3+}$ and $(C_{12}H_{28}N)_2CdBr_4:25\%Sb^{3+}$.

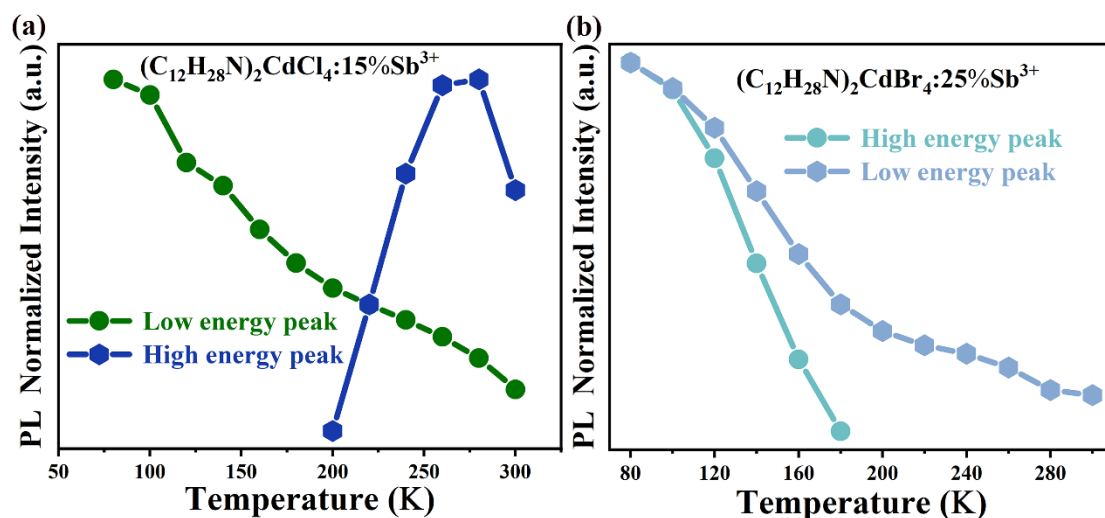


Figure S19. The emission intensity of (a) $(C_{12}H_{28}N)_2CdCl_4:15\%Sb^{3+}$ and (b) $(C_{12}H_{28}N)_2CdBr_4:25\%Sb^{3+}$ versus temperatures.

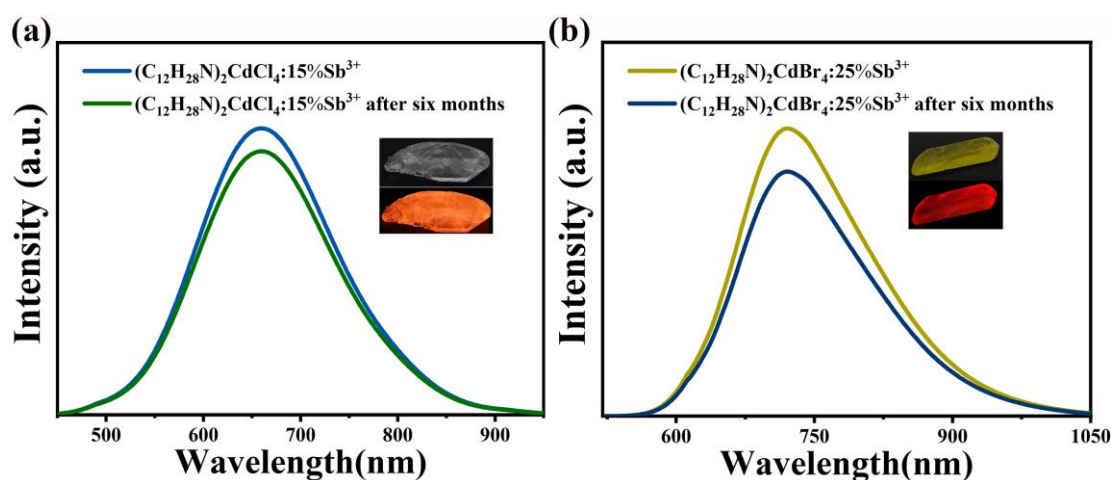


Figure S20. (a) PL spectra of $(C_{12}H_{28}N)_2CdCl_4:15\%Sb^{3+}$ and (b) $(C_{12}H_{28}N)_2CdBr_4:25\%Sb^{3+}$ before and after exposure to air for 6 months.

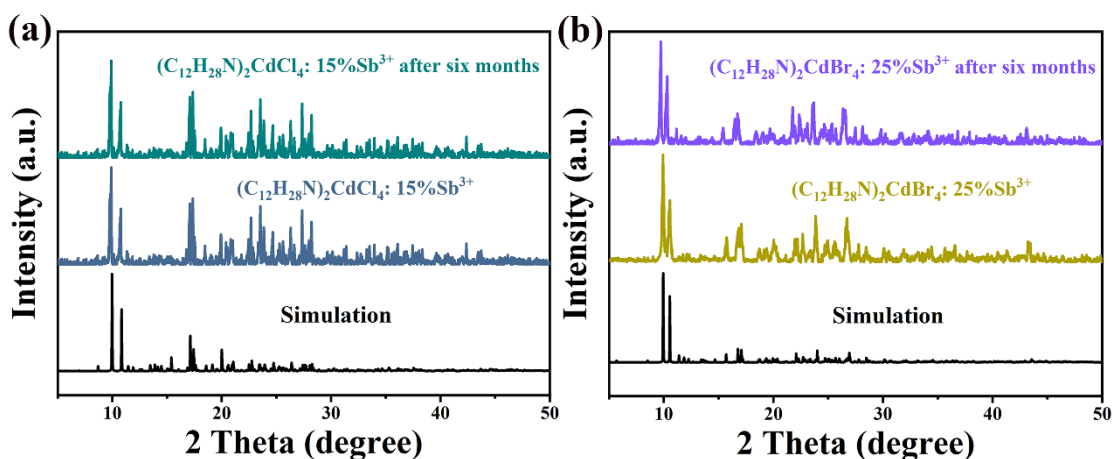


Figure S21. PXRD patterns of (a) $(C_{12}H_{28}N)_2CdCl_4:15\%Sb^{3+}$ and (b) $(C_{12}H_{28}N)_2CdBr_4:25\%Sb^{3+}$ before and after exposure to air for 6 months.

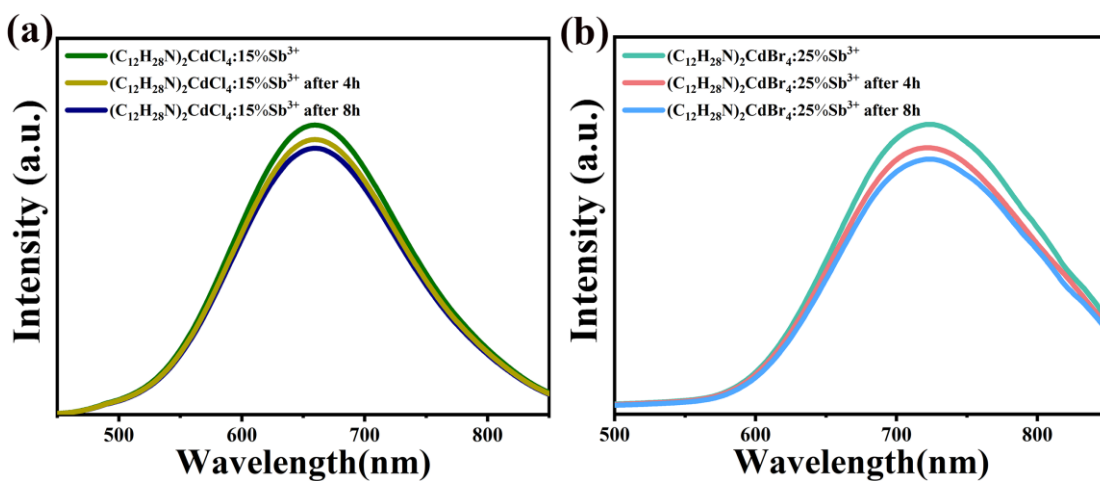


Figure S22. PL spectra of (a) $(C_{12}H_{28}N)_2CdCl_4:15\%Sb^{3+}$ and (b) $(C_{12}H_{28}N)_2CdBr_4:25\%Sb^{3+}$ before and after irradiation by 365 nm UV lamp for 4 h and 8 h.

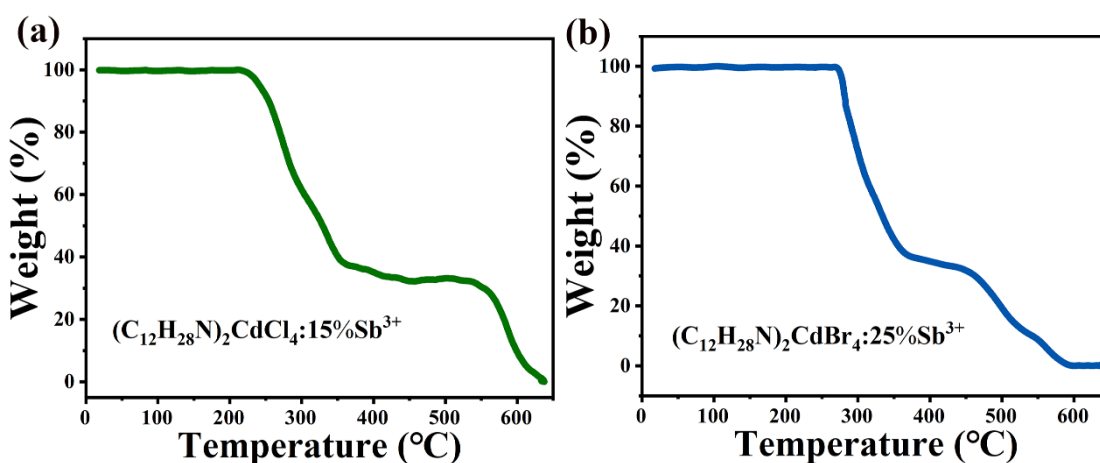


Figure S23. TGA curves of (a) 15%Sb³⁺-doped $(C_{12}H_{28}N)_2CdCl_4$ and (b) 15%Sb³⁺-doped $(C_{12}H_{28}N)_2CdBr_4$.

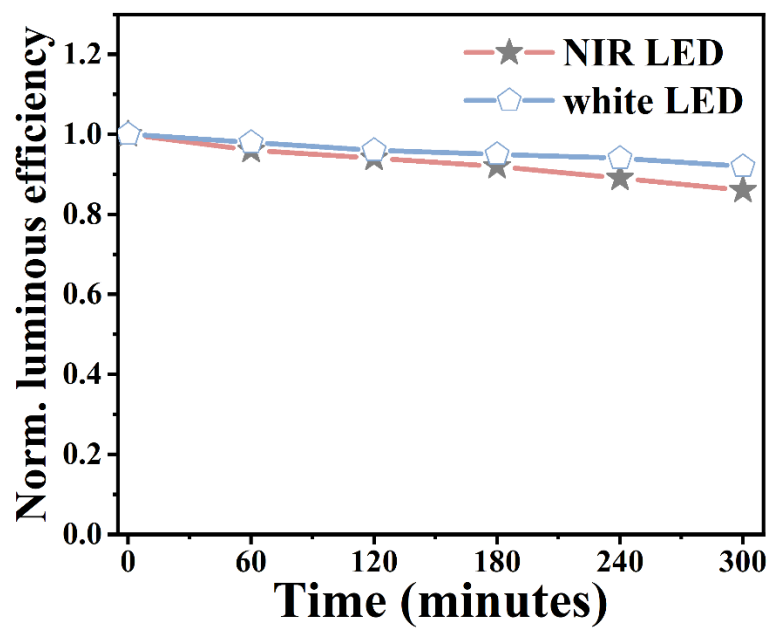


Figure S24. Long-time operational stability of NIR LED and white LED within 5h.

References

- [1] V. Morad, Y. Shynkarenko, S. Yakunin, A. Brumberg, R. D. Schaller, M. V. Kovalenko, *J. Am. Chem. Soc.* **2019**, 141, 9764.
- [2] B. Su, M. Li, E. Song, Z. Xia, *Adv. Funct. Mater.* **2021**, 31, 2105316.
- [3] X. Liu, X. Xu, B. Li, Y. Liang, Q. Li, H. Jiang, D. Xu, *CCS Chem.* **2020**, 2, 216.
- [4] Z. Li, G. Song, Y. Li, L. Wang, T. Zhou, Z. Lin, R.-J. Xie, *J. Phys. Chem. Lett.* **2020**, 11, 10164.
- [5] J. B. Luo, J. H. Wei, Z. Z. Zhang, Z. L. He, D. B. Kuang, *Angew. Chem., Int. Ed.* **2023**, 62, e202216504.
- [6] B. Li, J. Jin, M. Yin, X. Zhang, M. S. Molokeev, Z. Xia, Y. Xu, *Angew. Chem., Int. Ed.* **2022**, 61, e202212741.
- [7] G. Zhang, D. Wang, J. Ren, X. Zhou, Y. Wang, *Laser Photon. Rev.* **2023**, 17, 2300158.
- [8] B. Su, S. Geng, Z. Xiao, Z. Xia, *Angew. Chem., Int. Ed.* **2022**, 61, e202208881.
- [9] S. Yu, H. Peng, Q. Wei, T. Li, W. Huang, X. He, Z. Du, J. Zhao, B. Zou, *Mater. Horizons* **2024**, 11, 2230.
- [10] J. Wang, Z. Lyu, G. Peng, D. Sun, S. Shen, Z. Lu, L. Wang, H. Zhao, S. Wei, H. You, *Chem. Mat.* **2023**, 35, 3968.
- [11] X. Xu, Q. Shao, L. Yao, Y. Dong, J. Jiang, *Chem. Eng. J.* **2020**, 383.
- [12] Q. Zhang, X. Ding, X. Ma, Z. Su, B. Liu, Y. Wang, *Laser Photon. Rev.* **2024**, DOI: 10.1002/lpor.202400541.
- [13] H. Zhang, J. Zhong, C. Li, L. Wang, W. Zhao, *J. Lumines.* **2022**, 251.
- [14] Y. Wang, Z. Xu, M. Shang, Y. Sun, X. Xing, P. Dang, J. Lin, *Laser Photon. Rev.* **2024**, DOI: 10.1002/lpor.202400295.
- [15] C. Yang, D. Zheng, X. Zou, X. Dai, B. Tang, M. S. Molokeev, X. Zhang, H. Zhang, Y. Liu, B. Lei, *Adv. Opt. Mater.* **2024**, DOI: 10.1002/adom.202303235.
- [16] Z. Tang, F. Du, L. Zhao, H. Liu, Z. Leng, H. Xie, G. Zhang, Y. Wang, *Laser Photon. Rev.* **2023**, 17, 2200911.
- [17] Z. Tang, F. Du, H. Liu, Z. Leng, X. Sun, H. Xie, M. Que, Y. Wang, *Adv. Opt. Mater.* **2022**, 10, 2102204.
- [18] Z. Yang, Y. Zhao, Y. Zhou, J. Qiao, Y. C. Chuang, M. S. Molokeev, Z. Xia, *Adv. Funct. Mater.* **2021**, 32, 2103927.
- [19] J. Qiao, G. Zhou, Y. Zhou, Q. Zhang, Z. Xia, *Nat. Commun.* **2019**, 10, 5267.